Variational Bayes Phase Tracking for Correlated Dual-Frequency Measurements with Slow Dynamics

Stéphanie Bidon[a,*], Sébastien Roche[a]

[a] *Institut Supérieur de l'Aéronautique et de l'Espace, 10 av. Edouard Belin 31055 Toulouse, France*

Abstract

We consider the problem of estimating the absolute phase of a noisy signal when this latter consists of correlated dual-frequency measurements. This scenario may arise in many application areas such as global navigation satellite system (GNSS). In this paper, we assume a slow varying phase and propose accordingly a Bayesian filtering technique that makes use of the frequency diversity. More specifically, the method results from a variational Bayes approximation and belongs to the class of nonlinear filters. Numerical simulations are performed to assess the performance of the tracking technique especially in terms of mean square error and cycle-slip rate. Comparison with a more conventional approach, namely a Gaussian sum estimator, shows substantial improvements when the signal-to-noise ratio and/or the correlation of the measurements are low.

Keywords: Absolute phase tracking, phase unwrapping, cycle slips, multifrequency signal, nonlinear Bayesian filtering, variational Bayes approximation

1. Introduction

Over the last few decades signal phase measurement has become an active area of research. Indeed, in many applications, the carrier phase of a transmitted or reflected wave conveys information of primary interest to the operator. Phase measurement is directly related to surface height in interferometric synthetic aperture radar (InSAR) [1] and to the target radial velocity in radar [2] whereas in navigation it provides a highly-precise range measurement between the satellites and the receiver [3], to name a few examples.

Phase measurement is however by nature ambiguous. For instance, estimating the phase via a conventional four-quadrant inverse tangent leads to a wrapped observation in the principal interval $[-\pi, \pi]$. Without additional information, retrieving the absolute phase is thus an ill-posed problem.

*Corresponding author

Email addresses: stephanie.bidon@isae.fr (Stéphanie Bidon), sebastien.roche@isae.fr (Sébastien Roche)

To remove ambiguity, prior knowledge about the phase dynamics is usually injected into the estimation problem. For instance, in case of low value phase-gradient, an efficient unwrapping technique may be obtained simply by integrating the phase difference between two samples. However this method, which is based on restrictive assumptions [4], fails in case of noisy samples or when the phase dynamics increases locally and causes aliasing. Phase jumps, known also as cycle slips, arise then in the estimation process. A thorough description of this phenomenon can be found in [5] for phase-locked loops (PLL). To avoid cycle slips, more advanced techniques are usually required. Among them statistical modeling offers a flexible way to proceed. In particular, Markov random fields (MRF) have been widely used since they can guarantee a certain continuity between phase samples [6, 7, 8].

In addition to injecting prior knowledge about the phase dynamics, frequency diversity has been advocated as a complementary means for phase disambiguation [9]. Frequency diversity is obtained when the sensing system is able to observe the scene with different frequencies. The phase is then measured, up to a known frequency ratio, as many times as there are frequencies. The redundancy in the observations helps therefore to reduce cycle slips while reconstructing the absolute phase. This principle can be found in many application areas: in InSAR with the use of multiple interferograms [10], in radar with OFDM waveforms [11] or with the use of multiple pulse repetition frequencies [12], in navigation with the use of multifrequency receiver [13, 14, 15], in robotics with time-of-flights cameras [16], etc. Interestingly, a very related approach to remove phase ambiguity consists in using jointly the information conveyed by the envelope and the carrier frequency of the signal. Phase unwrapping techniques have been accordingly developed, e.g., in GNSS [17], in wideband radar [18] and for communication systems [19].

In this paper, we restrict our attention to dual-frequency measurements and propose in Section 2 a model to estimate the absolute phase for in-line processing applications. Particularly, the phase dynamics is assumed to be smooth enough to be represented by a first order MRF while some correlation is introduced between the amplitudes of both frequencies. Based on this model a Bayesian filtering technique is developed in Section 3. The method uses a variational Bayesian approximation [20] and results into a nonlinear filtering algorithm [21]. Numerical results are provided in Section 4 to illustrate the performance of the proposed absolute phase estimator. The latter is compared to a benchmark algorithm that belongs to a more conventional nonlinear filtering approach, namely a Gaussian sum estimator.

2. Signal Model

Herein we propose a signal model suited for correlated dual-frequency measurements. It is inspired mostly from [22] where a Bayesian approach is developed for absolute phase estimation in interferometric SAR. Our model is adapted here to take into account the proportional relationship residing between the two carrier phase measurements.

2.1. Measurement model

We consider the signal received on a single sensor that observes the same scene at two different carrier frequencies. The signal is demodulated with respect to (wrt) each carrier frequency on two independent RF chains. Assuming a unique and synchronized sampling rate, the baseband signal at the instant k can be expressed as

$$y_1(k) = \alpha_1(k)e^{j\phi(k)} + n_1(k)$$
$$y_2(k) = \alpha_2(k)e^{j\gamma\phi(k)} + n_2(k)$$

where

$(.)_{1,2}$ are subscripts that refer to the first and second frequencies (or channels) respectively;

$\alpha_{1,2}(k)$ is the received amplitude per channel;

$\phi(k)$ is the carrier phase of the first channel;

γ is the ratio between the second and first frequencies which are assumed ordered such that $\gamma > 1$;

$n_{1,2}(k)$ is the noise component per channel.

In the following, an equivalent vector notation is used for convenience, i.e.,

$$\boxed{\boldsymbol{y}_k = \boldsymbol{\alpha}_k \odot \begin{bmatrix} e^{j\phi_k} \\ e^{j\gamma\phi_k} \end{bmatrix} + \boldsymbol{n}_k} \tag{1}$$

where $\phi_k \triangleq \phi(k)$, $\odot$ is the Hadamard product and each 2-length vector gathers the information received on both channels, e.g., $\boldsymbol{y}_k = \begin{bmatrix} y_1(k) & y_2(k) \end{bmatrix}^T$.

2.1.1. Likelihood function

Due to the independence between the RF chains, the noise components $n_1(k)$ and $n_2(k)$ are modeled as independent random variables. Moreover, they are supposed to be identically distributed according to a classical Gaussian probability density function (pdf), viz

$$\boldsymbol{n}_k|\sigma_n^2 \sim \mathcal{CN}\left(\boldsymbol{0}, \sigma_n^2\boldsymbol{I}_2\right) \tag{2}$$

where σ_n^2 represents the noise power per sample per channel and $\boldsymbol{I}_2$ is the 2-by-2 identity matrix. The likelihood is thus given by

$$f(\boldsymbol{y}_k|\boldsymbol{\alpha}_k, \phi_k, \sigma_n^2) = \pi^{-2}\sigma_n^{-4} \exp\left\{-\sigma_n^{-2}\left\|\boldsymbol{y}_k - \boldsymbol{\alpha}_k \odot \begin{bmatrix} e^{j\phi_k} \\ e^{j\gamma\phi_k} \end{bmatrix}\right\|_2^2\right\} \tag{3}$$

where $\|.\|_2$ is the Frobenius norm. Note that, at this stage, the signal model (3) is not informative enough to define a maximum likelihood estimate of ϕ_k. In what follows, we propose to consider the measurement equation obtained from the marginalization of the likelihood function (3) over the nuisance parameter $\boldsymbol{\alpha}_k$. To do so, we need first to specify the distribution of the amplitude vector $\boldsymbol{\alpha}_k$.

2.1.2. Marginal likelihood function

Amplitude. The complex amplitudes $\alpha_1(k)$ and $\alpha_2(k)$ received by the sensor differ most likely from one another due to, for instance, some decorrelation process arising during propagation. A simple way to represent this decorrelation is to model the vector $\boldsymbol{\alpha}_k$ as a centered Gaussian random vector with the same power[1] σ_α^2 per channel and a correlation coefficient $\rho \in [0,1]$ between channels. This is denoted by

$$\boldsymbol{\alpha}_k|\sigma_\alpha^2, \rho \sim \mathcal{CN}\left(\mathbf{0}, \boldsymbol{R}_\alpha\right) \tag{4}$$

where the 2×2 matrix $\boldsymbol{R}_\alpha$ does not depend on k and is given by

$$\boldsymbol{R}_\alpha = \sigma_\alpha^2 \begin{pmatrix} 1 & \rho \\ \rho^* & 1 \end{pmatrix}.$$

The prior pdf of $\boldsymbol{\alpha}_k|\sigma_\alpha^2, \rho$ is thus given by

$$f(\boldsymbol{\alpha}_k|\sigma_\alpha^2, \rho) = \frac{1}{\pi^2 |\boldsymbol{R}_\alpha|} \exp\left\{-\boldsymbol{\alpha}_k^H \boldsymbol{R}_\alpha^{-1} \boldsymbol{\alpha}_k\right\}$$

where $|\boldsymbol{R}_\alpha| = \sigma_\alpha^4(1 - |\rho|^2)$.

Expression of the marginal likelihood function. Using (3) and (4) the marginal likelihood function can be obtained as

$$\begin{aligned} f(\boldsymbol{y}_k|\phi_k) &= \int f\left(\boldsymbol{y}_k|\boldsymbol{\alpha}_k, \phi_k\right) \; f(\boldsymbol{\alpha}_k) \; d\boldsymbol{\alpha}_k \\ &= \pi^{-2} |\boldsymbol{R}_{\boldsymbol{y}_k}|^{-1} \exp\left\{-\boldsymbol{y}_k^H \boldsymbol{R}_{\boldsymbol{y}_k}^{-1} \boldsymbol{y}_k\right\} \end{aligned}$$

where

$$\boldsymbol{R}_{\boldsymbol{y}_k} = \begin{pmatrix} \sigma_n^2 + \sigma_\alpha^2 & \sigma_\alpha^2 \rho e^{-j\tilde{\gamma}\phi_k} \\ \sigma_\alpha^2 \rho^* e^{j\tilde{\gamma}\phi_k} & \sigma_n^2 + \sigma_\alpha^2 \end{pmatrix} \tag{5}$$

with $\boxed{\tilde{\gamma} = \gamma - 1}$. It is still a Gaussian distribution, viz $\boldsymbol{y}_k|\phi_k \sim \mathcal{CN}\left(\mathbf{0}, \boldsymbol{R}_{\boldsymbol{y}_k}\right)$, that can be rewritten as follows

$$\begin{aligned} f(\boldsymbol{y}_k|\phi_k) \propto \exp&\left\{-\frac{(\sigma_n^2 + \sigma_\alpha^2)}{(\sigma_n^2 + \sigma_\alpha^2)^2 - |\rho|^2 \sigma_\alpha^4} \boldsymbol{y}_k^H \boldsymbol{y}_k\right\} \\ &\exp\left\{\beta_k \cos\left(\tilde{\gamma}\left[\frac{\varphi_k}{\tilde{\gamma}} - \phi_k\right]\right)\right\} \end{aligned} \tag{6}$$

where

$$\begin{cases} \beta_k = 2\dfrac{\sigma_\alpha^2}{[\sigma_n^2 + \sigma_\alpha^2]^2 - |\rho|^2 \sigma_\alpha^4} |z_k| \quad \text{and} \quad z_k = \rho y_1^*(k) y_2(k) \\ \varphi_k = \angle z_k \end{cases} \tag{7}$$

[1] For some applications, e.g., for GNSS multifrequency signals, this assumption may not be true. The model proposed should then be refined by assuming a channel dependent power.

with $\angle z_k = \arctan(\Im\{z_k\}/\Re\{z_k\})$ the angle of z_k that lies between $[-\pi, +\pi]$. $\Re\{\}$ and $\Im\{\}$ denote respectively the real and imaginary parts. Note that in (6) the parameter $\varphi_k/\tilde{\gamma}$ is *a* marginal maximum likelihood (MML) estimate of the absolute phase ϕ_k and lies in the interval $\left[-\frac{\pi}{\tilde{\gamma}}, +\frac{\pi}{\tilde{\gamma}}\right]$. In the remaining, it is denoted as

$$\boxed{\hat{\psi}_k^{\text{mml}} \triangleq \frac{\varphi_k}{\tilde{\gamma}}}. \tag{8}$$

Distributions of $\hat{\psi}_k^{mml}$ and β_k. Before continuing to describe the signal model, it is worth noticing from (6) that the measurement of interest is entirely described by the parameter z_k in (7), which is (up to the factor ρ) the product of the signal received on both frequencies. As a consequence, the performance of the absolute phase estimator proposed in the next Section will strongly depend on the distribution of z_k. More specifically, it will be useful to know the joint distribution of $\beta_k, \hat{\psi}_k^{\text{mml}}|\phi_k$ as well as the distributions of $\beta_k|\phi_k$ and $\hat{\psi}_k^{\text{mml}}|\phi_k$. Using results gathered in [23], the following expressions can be obtained

$$f(\beta_k, \hat{\psi}_k^{\text{mml}}|\phi_k) = \frac{\tilde{\gamma}}{2\pi}\frac{1-|\varrho|^2}{|\varrho|^2}\beta_k \exp\left\{\beta_k \cos\left(\tilde{\gamma}[\hat{\psi}_k^{\text{mml}} - \phi_k]\right)\right\} K_0\left\{\frac{\beta_k}{|\varrho|}\right\} \tag{9a}$$

$$f(\hat{\psi}_k^{\text{mml}}|\phi_k) = \frac{\tilde{\gamma}}{2\pi}\frac{1-|\varrho|^2}{(1-c^2)}\left[1 - \frac{c\arccos(c)}{\sqrt{1-c^2}}\right]\mathbb{I}_{\left[-\frac{\pi}{\tilde{\gamma}}, \frac{\pi}{\tilde{\gamma}}\right]}(\hat{\psi}_k^{\text{mml}}) \tag{9b}$$

$$f(\beta_k|\phi_k) = \frac{1-|\varrho|^2}{|\varrho|^2} I_0\{\beta_k\} K_0\left\{\frac{\beta_k}{|\varrho|}\right\} \tag{9c}$$

where $c = -|\varrho|\cos\left(\tilde{\gamma}[\hat{\psi}_k^{\text{mml}} - \phi_k]\right)$ and

$I_q\{\}, K_q\{\}$ are the modified Bessel functions of, respectively, the first and second kind at the qth order;

$\mathbb{I}_{\mathcal{I}}()$ denotes the indicator function of the set $\mathcal{I}$, (i.e., $\mathbb{I}_{\mathcal{I}}(x) = 1$ if $x \in \mathcal{I}$ and $\mathbb{I}_{\mathcal{I}}(x) = 0$ otherwise).

In (9), ϱ is the correlation coefficient associated with the 2-length vector $\boldsymbol{y}_k|\phi_k$. According to (5), its modulus is

$$\boxed{|\varrho| = \frac{|\rho|}{1 + SNR^{-1}}} \tag{10}$$

with SNR being the signal-to-noise ratio defined as

$$\boxed{SNR = \frac{\sigma_\alpha^2}{\sigma_n^2}}.$$

It is already interesting to note that the joint distribution (9a) depends only on the phase process ϕ_k and the parameters $\tilde{\gamma}$ and $|\varrho|$; the latter being the actual correlation coefficient between the two carrier frequencies weighted by the SNR. We see in Fig. 1 that $|\varrho|$ is always less than $|\rho|$ and can be strongly degraded by a low SNR.

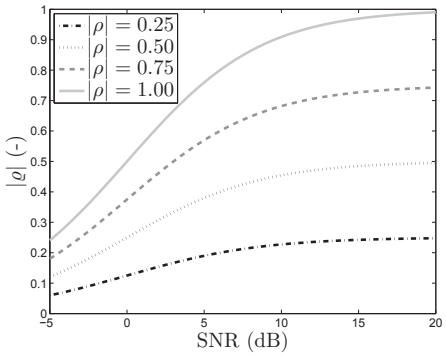

Figure 1: Correlation coefficient $|\varrho|$ (10) as a function of the SNR.

2.2. Phase process

We continue herein to describe the signal model and discuss to that end the phase process. Since we are interested in estimating the *absolute* phase ϕ_k recursively in time, it is necessary to assume a phase dynamic model that, hopefully, will avoid any ambiguity to arise during estimation (i.e., no cycle slip). To that end, the phase evolution is modeled by a Markov random field. Here, we assume a first order Gaussian MRF to ensure a certain smoothness for the phase from sample $k-1$ to k [8]. A causal distribution is considered since our primary interest is devoted to inline processing. More specifically, the initial state ϕ_1 is supposed to be uniformly distributed over a symmetric set $\mathcal{I}$ while the phase at time $k > 1$ is thought to be Gaussian distributed with mean ϕ_{k-1} and variance σ_ϕ^2, i.e.,

$$\phi_1 \sim \mathcal{U}_\mathcal{I} \tag{11a}$$

$$\phi_k|\phi_{k-1} \sim \mathcal{N}\left(\phi_{k-1}, \sigma_\phi^2\right) \tag{11b}$$

which leads to the following distributions

$$f(\phi_1) \propto \mathbb{I}_\mathcal{I}\left(\phi_1\right) \tag{12a}$$

$$f(\phi_k|\phi_{k-1}, \sigma_\phi^2) = \frac{1}{\sqrt{2\pi\sigma_\phi^2}} \exp\left\{-\frac{\left[\phi_k - \phi_{k-1}\right]^2}{2\sigma_\phi^2}\right\}. \tag{12b}$$

Values for the endpoints of the interval $\mathcal{I}$ is discussed later in Section 3.2. Note also that the parameter σ_ϕ^2 monitors the degree of smoothness of the unwrapped phase.

2.3. Hyperparameters

In this work, the parameters σ_n^2, σ_α^2, ρ and σ_ϕ^2 are supposed to be deterministic known constants[2].

3. Restricted variational Bayesian filtering

3.1. Bayesian filtering formulation

Equations (6) and (11) form a conventional Bayesian filtering problem where the former equation defines the measurement model and the latter represents the dynamic model. The optimal filtering is tantamount to recursively estimating in two stages the filtering distribution $f(\phi_k|\boldsymbol{Y}_k)$ where $\boldsymbol{Y}_k = \begin{bmatrix}\boldsymbol{y}_1 & \dots & \boldsymbol{y}_k\end{bmatrix}$ as follows [24]

- Time update

$$f(\phi_1|\boldsymbol{Y}_0) \triangleq f(\phi_1) \qquad (k=1)$$
$$f(\phi_k|\boldsymbol{Y}_{k-1}) = \int f(\phi_k|\phi_{k-1}) f(\phi_{k-1}|\boldsymbol{Y}_{k-1}) d\phi_{k-1} \qquad (k>1)$$

  where the subscript $_0$ denotes the set of no measurements

- Data update

$$f(\phi_k|\boldsymbol{Y}_k) \propto f(\boldsymbol{y}_k|\phi_k) f(\phi_k|\boldsymbol{Y}_{k-1}) \qquad (k \geq 1)$$

Given the state space model (6)-(11), the optimal filtering seems intractable and one is left with evaluating suboptimal filtering distribution [21]. We propose to use herein a restricted variational Bayes (RVB) approximation [20]. As shown in what follows, this approach allows the nonlinear nature of the measurement equation to be preserved and leads to explicit expression of the filtering distribution which is very attractive on the implementation point of view.

3.2. Principle of the RVB filtering

The RVB-based method proposed stems from two approximations introduced in the optimal filtering problem. Following [20] a local variational approximation is firstly made. Applied to our model, it consists in imposing that the phases ϕ_k and ϕ_{k-1} are independent conditionally to $\boldsymbol{Y}_k$. Using the variational Bayes approximation leads then to recursively evaluating an approximate filtering distribution $\tilde{f}(\phi_k|\boldsymbol{Y}_k)$ as follows [20]

[2]Constant terms are omitted in the conditional terms in the remaining of the paper for notational convenience.

- Time update

$$\tilde{f}(\phi_k|\boldsymbol{Y}_{k-1}) \propto \exp\left\{\langle \log\left(f(\phi_k|\phi_{k-1})\right)\rangle_{\tilde{f}(\phi_{k-1}|\boldsymbol{Y}_k)}\right\}$$

with

$$\tilde{f}(\phi_{k-1}|\boldsymbol{Y}_k) \propto \exp\left\{\langle \log\left(f(\phi_k|\phi_{k-1})\right)\rangle_{\tilde{f}(\phi_k|\boldsymbol{Y}_k)}\right\} \tilde{f}(\phi_{k-1}|\boldsymbol{Y}_{k-1})$$

- Data update

$$\tilde{f}(\phi_k|\boldsymbol{Y}_k) \propto f\left(\boldsymbol{y}_k|\phi_k\right)\ \tilde{f}(\phi_k|\boldsymbol{Y}_{k-1}) \tag{13}$$

where $\langle g(\theta)\rangle_{f(\theta)} = \int g(\theta) f(\theta) d\theta$ is the expectation value of the function $g(\theta)$ wrt the distribution $f(\theta)$. Then, to make the filtering problem tractable, a second approximation is introduced [20]. The distribution $\tilde{f}(\phi_{k-1}|\boldsymbol{Y}_k)$, which depends itself "undesirably" on the approximate posterior pdf $\tilde{f}(\phi_k|\boldsymbol{Y}_k)$, is replaced with the fixed variational Bayes (VB) distribution $\tilde{f}(\phi_{k-1}|\boldsymbol{Y}_{k-1})$ so that the time and data update stages become respectively

$$\begin{aligned}
\tilde{f}(\phi_k|\boldsymbol{Y}_{k-1}) &\propto \exp\left\{\langle \log\left(f(\phi_k|\phi_{k-1})\right)\rangle_{\tilde{f}(\phi_{k-1}|\boldsymbol{Y}_{k-1})}\right\} \\
\tilde{f}(\phi_k|\boldsymbol{Y}_k) &\propto f\left(\boldsymbol{y}_k|\phi_k\right)\ \tilde{f}(\phi_k|\boldsymbol{Y}_{k-1}).
\end{aligned}$$

Using (6) and (11), the RVB filtering can be finally formulated as

- Time and data updates for $k = 1$

$$\tilde{f}(\phi_1|\boldsymbol{Y}_0) \triangleq f(\phi_1) \tag{14a}$$

$$\tilde{f}(\phi_1|\boldsymbol{Y}_1) \propto f(\phi_1) \exp\left\{\beta_1 \cos\left(\tilde{\gamma}[\hat{\psi}_1^{\mathrm{mml}} - \phi_1]\right)\right\} \tag{14b}$$

- Time and data updates for $k > 1$

$$\phi_k|\boldsymbol{Y}_{k-1} \underset{\tilde{f}}{\sim} \mathcal{N}\left(\langle\phi_{k-1}\rangle_{\tilde{f}(\phi_{k-1}|\boldsymbol{Y}_{k-1})}, \sigma_\phi^2\right) \tag{15a}$$

$$\tilde{f}(\phi_k|\boldsymbol{Y}_k) \propto \exp\left\{\beta_k \cos\left(\tilde{\gamma}[\hat{\psi}_k^{\mathrm{mml}} - \phi_k]\right) - \frac{\left[\phi_k - \langle\phi_{k-1}\rangle_{\tilde{f}(\phi_{k-1}|\boldsymbol{Y}_{k-1})}\right]^2}{2\sigma_\phi^2}\right\}. \tag{15b}$$

Thanks to the RVB approximation, the functional forms of both the prediction and filtering distributions are now preserved from one iteration to another [20].

In light of the expression (14b) we set $\mathcal{I} = [-\pi/\tilde{\gamma}; \pi/\tilde{\gamma}]$ which ensures that the VB filtering distribution at $k = 1$ lies in the family of the Tikhonov (or von Mises [25]) distribution thereby facilitating the derivation of $\hat{\phi}_1^{\mathrm{rvb}}$.
Additionally it is worth noticing that for $k > 1$ the functional form of the VB

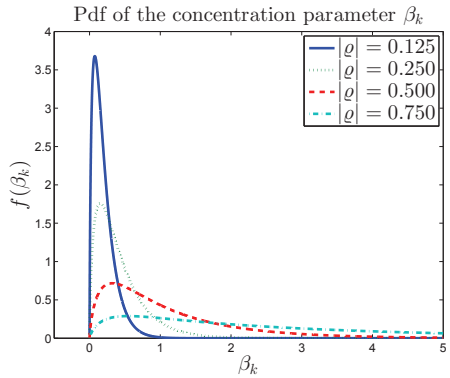

Figure 2: Pdf of the concentration parameter β_k in (9c) for different value of $|\varrho|$.

filtering distribution (15b) has been encountered in other statistical phase unwrapping problems, e.g., [26, 6, 22]. It is a periodic function that, restricted to one period, is the product of a von Mises distribution[3] (with mean direction $\hat{\psi}_k^{\text{mml}}$ and concentration parameter β_k) and a Gaussian distribution (with mean $\langle \phi_{k-1} \rangle_{\tilde{f}(\phi_{k-1}|\boldsymbol{Y}_{k-1})}$ and variance σ_ϕ^2). Due to the periodic component, multiple modes can arise when $\beta_k \tilde{\gamma}^2 \sigma_\phi^2 > 1$ (see Appendix A where the exact number of modes and their location within an interval are given in closed form). Conventionally, to deal with this possible multimodality, techniques based on Gaussian sum approximations are developed [27]. For instance in [26, 6], the von Mises distribution is approximated by a train of Gaussian functions. If this scheme is precise enough for high concentration parameters β_k, it is much less accurate for lower values of β_k [25, p.38]. Practically, the latter case will most likely happen when the correlation coefficient $|\varrho|$ (10) is low (see Fig. 2) or equivalently whenever $|\rho|$ or the SNR is low (see Fig. 1). As a consequence we propose to pursue designing our estimation scheme while using the filtering distribution as it is.

3.3. RVB estimator

The recursive propagation of the posterior density, given by (14)-(15), requires exclusively the evaluation of the mean of ϕ_k wrt to the VB filtering distribution $\tilde{f}(\phi_k|\boldsymbol{Y}_k)$. In other words, to obtain the filtering distribution, it is necessary and sufficient to derive the minimum mean square error (MMSE) estimator of ϕ_k wrt to the VB posterior. The latter is referred in the following to as the RVB estimator

$$\hat{\phi}_k^{\text{rvb}} \triangleq \langle \phi_k \rangle_{\tilde{f}(\phi_k|\boldsymbol{Y}_k)} = \int \phi_k \tilde{f}(\phi_k|\boldsymbol{Y}_k) d\phi_k. \tag{16}$$

[3] Up to the scale parameter $\tilde{\gamma}$.

Note that once (16) is derived, the entire VB filtering distribution is known and one could define other estimators, e.g., the maximum a posteriori (MAP) estimator. In any event, one should focus its attention first on the evaluation of (16). It is shown in Appendix B and Appendix C that the RVB estimator can be expressed as an infinite discrete sum as follows, for $k = 1$

$$\boxed{\hat{\phi}_1^{\text{rvb}} = \frac{2}{\tilde{\gamma}} \sum_{q=1}^{+\infty} (-1)^{q+1} \frac{I_q\{\beta_1\}}{I_0\{\beta_1\}} \frac{\sin(q\tilde{\gamma}\hat{\psi}_1^{\text{mml}})}{q}} \tag{17}$$

and for $k > 1$

$$\boxed{\hat{\phi}_k^{\text{rvb}} = \hat{\phi}_{k-1}^{\text{rvb}} + 2\tilde{\gamma}\sigma_\phi^2 \frac{\sum_{q=1}^{\infty} q I_q\{\beta_k\} \sin\left(q\tilde{\gamma}[\hat{\psi}_k^{\text{mml}} - \hat{\phi}_{k-1}^{\text{rvb}}]\right) e^{-\frac{\sigma_\phi^2 \tilde{\gamma}^2 q^2}{2}}}{I_0\{\beta_k\} + 2\sum_{q=1}^{\infty} I_q\{\beta_k\} \cos\left(q\tilde{\gamma}[\hat{\psi}_k^{\text{mml}} - \hat{\phi}_{k-1}^{\text{rvb}}]\right) e^{-\frac{\sigma_\phi^2 \tilde{\gamma}^2 q^2}{2}}}.} \tag{18}$$

In practice, since $I_q\{x\}$ decreases rapidly wrt $I_0\{x\}$ when q increases for all x, we propose to implement a truncated version of (17) and (18) where the index q varies in a given interval $\{1, \ldots, q_{\max}\}$.

From (17) and (18) it is worth noticing that the RVB approximation yields a nonlinear algorithm that estimates the absolute phase ϕ_k via the use of not only the wrapped phase $\angle z_k$ but also the modulus $|z_k|$ where $z_k \triangleq \rho y_1^*(k) y_2(k)$ has been defined in (7). In other words, the RVB estimator uses the measurement of both the phase difference and the product of the amplitude between the two carriers. Furthermore from (18) one can appreciate the nonlinear nature of the RVB estimator updating compared for instance to a conventional Kalman filter [21].

Remark 1 (Implementation of the RVB estimator). To avoid numerical problems one should use at high SNR (where β_k can have large values) a scaled version of the modified Bessel function, i.e., $I_q\{\beta_k\}\exp(-\beta_k)$ [28]. Furthermore, very rarely the denominator of (18) becomes very small numerically. This case may arise when $\hat{\phi}_{k-1}^{\text{rvb}}$ is approximately halfway between the two nearest modes of $\exp(\beta_k \cos(\tilde{\gamma}[\hat{\psi}_k^{\text{mml}} - \phi_k]))$. In that case, we replace locally the RVB estimator by the MAP estimator. The latter can be derived with standard optimization algorithms since the number of modes and their location within an interval are known (see Appendix A).

4. Numerical simulations

We now present various numerical examples illustrating the performance of the RVB estimator and the role that the process noise power σ_ϕ^2 plays. In the remaining, data are generated according to the model (1), (2) and (4). The truncation value $q_{\max} = 50$ is chosen to implement (18) as it offers a convenient, though not optimized, compromise between the computation load and the truncation error induced in the RVB estimator (18) for a wide variety of scenarii.

4.1. Observation of single realizations

To gain some insight into the behavior of the RVB estimator (18), its response is depicted in Figure 3 for a single realization when the phase input is successively a step, a ramp or an acceleration. Typical behavior pertaining to absolute phase estimators can be observed. First, the estimator requires a certain amount of time to obtain lock. This is well illustrated on the phase step response, where about 150 samples are needed for the absolute value of the phase error process, namely $\epsilon_k^{\mathrm{rvb}} \triangleq \phi_k - \hat{\phi}_k^{\mathrm{rvb}}$, to remain under a certain threshold. From the acquisition mode, the process enters then the tracking mode. Secondly, the phenomenon of cycle slipping is well identifiable: for instance, on the phase ramp-response, the RVB estimator loses its equilibrium around the 700-th sample and the phase error process augments by one cycle before returning to steady-state. Note that for the acceleration input the estimator constantly skips cycles beyond a given time. This is expectable since the RVB estimator (18) is designed, so far, for a first order dynamics and cannot endure an increasing variance. In the remaining, we will mainly focus our attention to step- and ramp-responses, i.e., otherwise stated the absolute phase process will have the following functional form: $\phi_k = \phi_0 + \dot{\phi}_0 k$ where ϕ_0 and $\dot{\phi}_0$ are respectively the initial phase and initial phase rate.

4.2. Performance metrics

To assess more precisely the performance of the proposed RVB algorithm, the statistical behavior of the phase error process $\epsilon_k^{\mathrm{rvb}}$ is studied as for any absolute phase estimator [29, 30, 31]. To that end, three classical metrics are considered, namely [32]:

- the acquisition time; evaluated here as the time necessary for the modulo-$2\pi/\tilde{\gamma}$ error phase process to attain a constant root mean square error (RMSE);
- the precision of estimation; evaluated here by the RMSE of the modulo-$2\pi/\tilde{\gamma}$ error phase process (denoted as RMSE-mod);
- the cycle slip rate which is the average number of cycle slips per track; in our simulations a cycle slip is said to be detected as soon as the phase error crosses a new equilibrium line $2p\pi/\tilde{\gamma}$, $p \in \mathbb{Z}$.

Though the expression of the RVB estimator (17)-(18) and that of the joint pdf of $\beta_k, \hat{\psi}_k^{\mathrm{mml}} | \phi_k$ (9a) are known explicitly, the calculation in closed form of these three metrics seems intricate. We thus turn to numerical simulations and use 5000 Monte-Carlo runs. Nevertheless, from the expressions (17)-(18) and (9a), we can conclude beforehand that the performance of the RVB estimator depends only on the phase process ϕ_k, the ratio frequency γ, the process noise power σ_ϕ^2 and the correlation coefficient $|\varrho|$ defined in (10). In the remaining, the studied scenarii are thus described wrt the parameter $|\varrho|$ instead of the pair (ρ, SNR); keeping in mind that a given value of $|\varrho|$ refers to an infinite number of scenarii where (ρ, SNR) verifies the formula (10) (see also Fig.1). Furthermore, as for

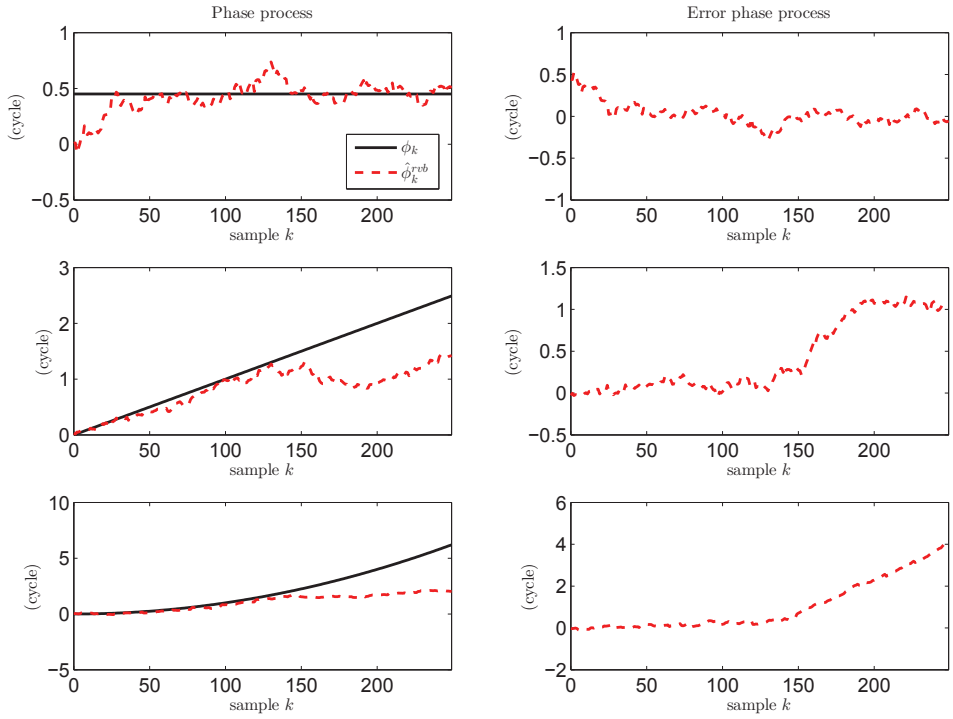

Figure 3: Phase responses of the RVB estimator to a step-, ramp- and acceleration-input: (left column) phase process ϕ_k and $\hat{\phi}_k^{\text{rvb}}$; (right column) phase error process $\phi_k - \hat{\phi}_k^{\text{rvb}}$. One cycle corresponds to $2\pi/\tilde{\gamma}$ radians. $|\varrho| \approx 0.25$ (e.g., SNR=0 dB, $\rho = 0.5$), $\gamma = 1.25$, $\sigma_\phi = 0.8$ half-cycle.

any Bayesian filtering technique, the tuning of the process noise power σ_ϕ^2 is a very important task. Therefore, in the next two Sections performance of the RVB estimator is displayed as a function of this parameter[4] so as to give a mean to select adequately its value in practice.

Finally, note that the proposed RVB estimator is implemented jointly with the Gaussian sum (GS) estimator proposed in [26] for comparison purposes (the so-called multiplication, agglutination and elimination parameters have been set respectively to 3, $(0.1 \times 2\pi/\tilde{\gamma})^{1/2}$, and 0.01 according to [26, 6]). We can already underline that in terms of computational complexity the RVB technique presents advantages over the GS method. Indeed, according to (18), implementing the former requires only basic operations (e.g., sum, division, use of modified Bessel functions that have efficient routines [33]) whereas the latter entails a time consuming procedure to keep the filter dimension within reasonable limits.

[4]To facilitate the interpretation σ_ϕ is expressed in the graphs in half-cycle (h.c.), i.e., $\sigma_\phi/(\pi/\tilde{\gamma})$.

4.3. Phase-step response

Fig. 4 shows the evolution of the RMSE of the modulo $2\pi/\tilde{\gamma}$ process wrt to the time for a phase-step input. For both the RVB and GS estimators, it can be observed that the RMSE-mod reaches a constant value after a given time and this for each value of σ_ϕ considered. This acquisition time is assessed numerically and is represented as a function of the standard deviation σ_ϕ in Fig. 5(a). The RMSE-mod at steady state is also depicted in Fig. 5(b) as well as the cycle slipping rate in Fig. 5(c). From these curves, we see that the RVB estimator attains lower RMSEs at steady state and much lower cycle slip rates than the Gaussian sum estimator. However, this is most of the time at the price of a slower convergence. Nonetheless, contrary to the Gaussian sum approach, the RVB can, subject to an appropriate choice for the value σ_ϕ, offer an appealing compromise wrt the three metrics under consideration. For instance, in this scenario with low correlation coefficient $|\varrho|$, the value $\sigma_\phi = 0.2$ cycle or $\sigma_\phi = 0.7$ cycle is a suitable choice to obtain in a few samples a precise phase estimator that has a probability of cycle slip near to zero. In any event, it is worth noticing that the performance of the RVB estimator is much less sensitive to the tuning of the process noise power σ_ϕ^2 than the GS estimator. Particularly, it is interesting to acknowledge the behavior of the RVB estimator wrt the parameter σ_ϕ: both RMSE-mod, cycle-slip rate and convergence rate decrease when either σ_ϕ tends to zero or increases towards infinity. A possible explanation is that the process noise power σ_ϕ appears in two opposite ways in (18):

1. as a multiplicative term that tends to reduce the contribution of the innovation when σ_ϕ decreases (in that case σ_ϕ^2 plays a similar role to that of the loop bandwidth of a PLL);
2. in an exponential term that tends to reduce the contribution of the innovation when σ_ϕ increases.

The scenario studied so far in Figs. 4 and 5 corresponds to a challenging setup where the actual coefficient correlation $|\varrho|$ is low (i.e., when the SNR and/or the correlation coefficient $|\rho|$ are low). To assess the influence of this parameter, Figs. 6 and 7 depict the performance of the RVB and GS estimators for higher values of $|\varrho|$. Increasing $|\varrho|$ leads all in all to higher convergence rate, lower RMSE-mod and lower cycle slipping rate for both estimators. Furthermore, it is important to note that the benefit of the proposed RVB method compared to the GS approach is then less pronounced. This result may be expectable since the approximation of the von Mises distribution, appearing in the filtering pdf (15b), by a train of Gaussian functions becomes very accurate for high concentration parameter β_k; which arises most likely when $|\varrho|$ comes close to 1 (see end of Section 3.2).

4.4. Phase-ramp response

In the last Section we have observed that, in case of a phase-step process, the RVB estimator is more performant than the GS approach especially when the actual coefficient correlation $|\varrho|$ is low. Herein we extend the performance

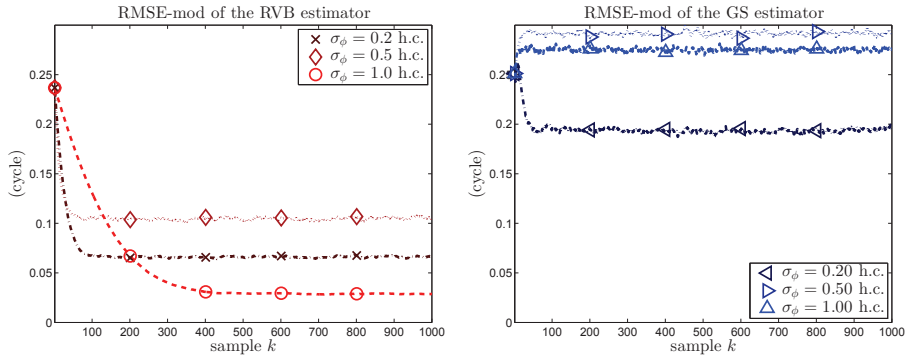

(a) (b)

Figure 4: RMSE-mod as a function of the time index for a phase-step process. $|\varrho| \approx 0.25$ (e.g., SNR=30 dB, $\rho = 0.25$), $\gamma = 1.25$, $\phi_0 = .25$ cycle, $\dot{\phi}_0 = 0$ cycle/sample. (a) Proposed RVB estimator. (b) GS estimator of [26].

study to a phase-ramp process. Contrary to a phase-step input and though not depicted in this paper, we can observe that for some values of σ_ϕ^2 the RMSE-mod of both estimators has an oscillatory behavior wrt to the time. In other words, for certain values of the process noise power, the phase estimator never gets in lock. For instance, if σ_ϕ^2 is too small the contribution of the innovation is then too limited to compensate for the phase rotation taking place during the estimator updating. As a consequence, we choose to concentrate our attention mostly on the cycle slipping rate metric and depict also the RMSE-mod wrt to the time for some values of σ_ϕ^2 where lock has been obtained. From Figs. 8, 9 and 10, we can see that for both estimators there is a distinct range of values σ_ϕ^2 for which the cycle slipping rate is significantly lower than everywhere else. This range is roughly located in the interval $[\dot{\phi}_0, \pi/\tilde{\gamma}]$ (rad). Outside this range, the prediction pdf (15a) is either not enough broaden (i.e., σ_ϕ^2 is too small) or too much broaden (i.e., σ_ϕ^2 is too large) to ensure a correct data update and thus a correct estimation. Note that for both estimators, the lower the correlation coefficient $|\varrho|$, the narrower this range. Moreover, it is worth noticing that the RVB technique offers again lower cycle slipping rate and lower RMSE-mod compared to the GS approach. As in the case of a phase-step input, the benefit of the RVB estimator is more perceivable for low correlation coefficient $|\varrho|$.

4.5. Phase response for GNSS applications

To finish, we present results when the phase process ϕ_k is generated according to a realistic GNSS scenario while the rest of the signal is still generated according to the model (1), (2) and (4). More specifically, the signal received on a GPS-receiver is synthetized with a realistic satellite-to-receiver dynamics. The phase to be tracked is then obtained as the angle of the prompt correlator of a conventional DLL-FLL (Delay Lock Loop/Frequency Lock Loop) [3,

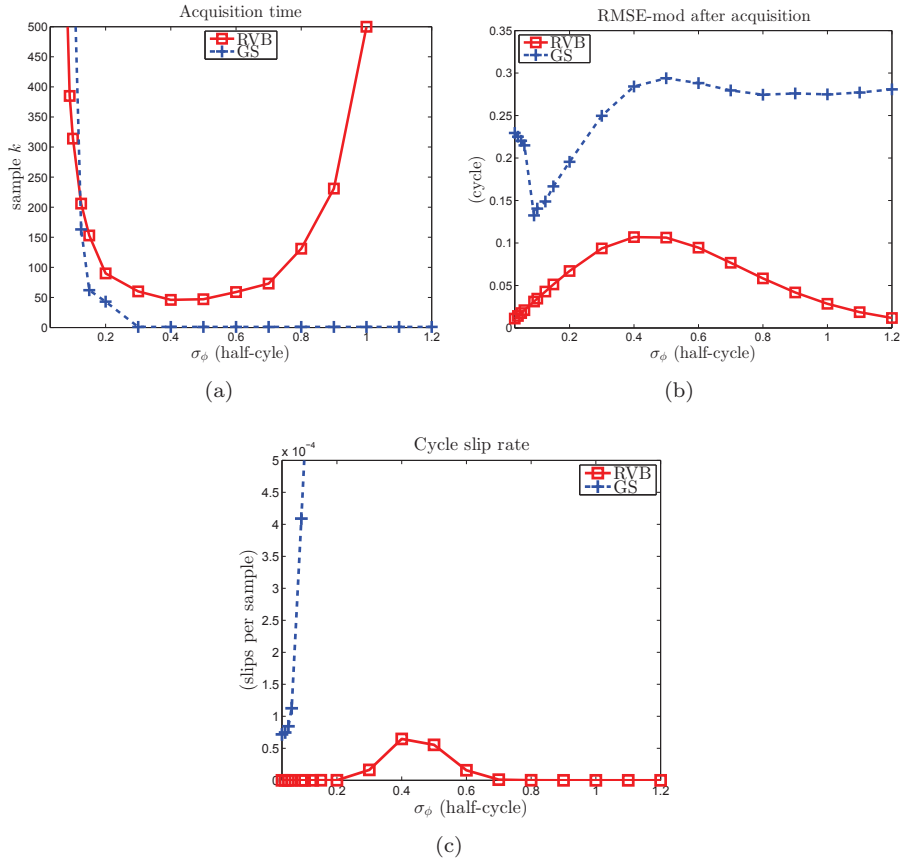

Figure 5: Performance of the proposed RVB estimator and the GS estimator of [26] for a phase-step process. $|\varrho| \approx 0.25$ (e.g., SNR=30 dB, $\rho = 0.25$), $\gamma = 1.25$, $\phi_0 = .25$ cycle, $\dot{\phi}_0 = 0$ cycle/sample. (a) Acquisition time. (b) RMSE-mod after acquisition. (c) Cycle slip rate.

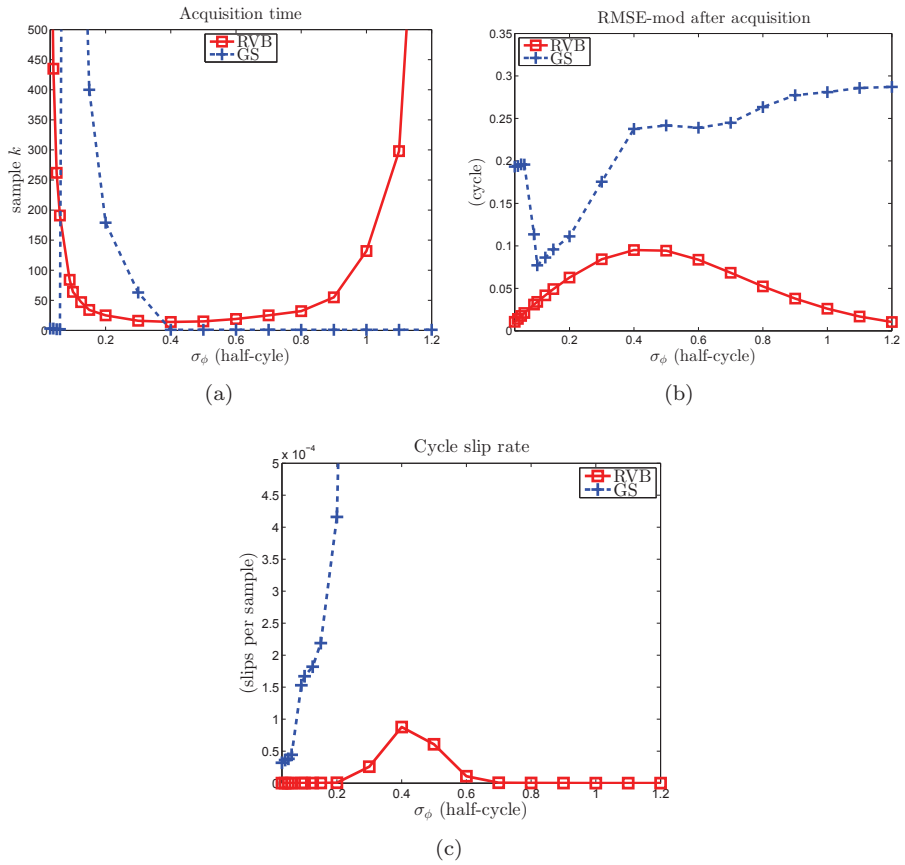

Figure 6: Performance of the proposed RVB estimator and the GS estimator of [26] for a phase-step process. $|\varrho| \approx 0.5$ (e.g., SNR=30 dB, $\rho = 0.5$), $\gamma = 1.25$, $\phi_0 = .25$ cycle, $\dot{\phi}_0 = 0$ cycle/sample. (a) Acquisition time. (b) RMSE-mod after acquisition. (c) Cycle slip rate.

ch.5]. The latter remains in lock during the whole estimation process. In GNSS applications, signals are emitted in the L band. Herein two conventional frequencies are considered namely the $L_1 = 1575.42$ MHz (frequency for which the received signal is synthetized) and $L_2 = 1227.6$ MHz frequencies so that the carrier frequency ratio is $\gamma = f_{L1}/f_{L2} \approx 1.28$. The signal-to-noise density ratio and the correlation time of the DLL-FLL are chosen respectively as $CN0 = 17$ dBHz and $T = 20$ ms which is equivalent to a signal-to-noise ratio equal to SNR=$CN0 \times T = 0$ dB. The SNR is assumed to be identical on both frequencies whereas the delay introduced by the ionosphere between the two frequencies is assumed to be compensated for. Finally, the level of correlation between the two frequencies is assumed to be equal to $\rho = 0.9$.

Fig. 4.5 depicts the true phase process as well as the phase estimated by the proposed RVB algorithm and that of the GS method. The process noise

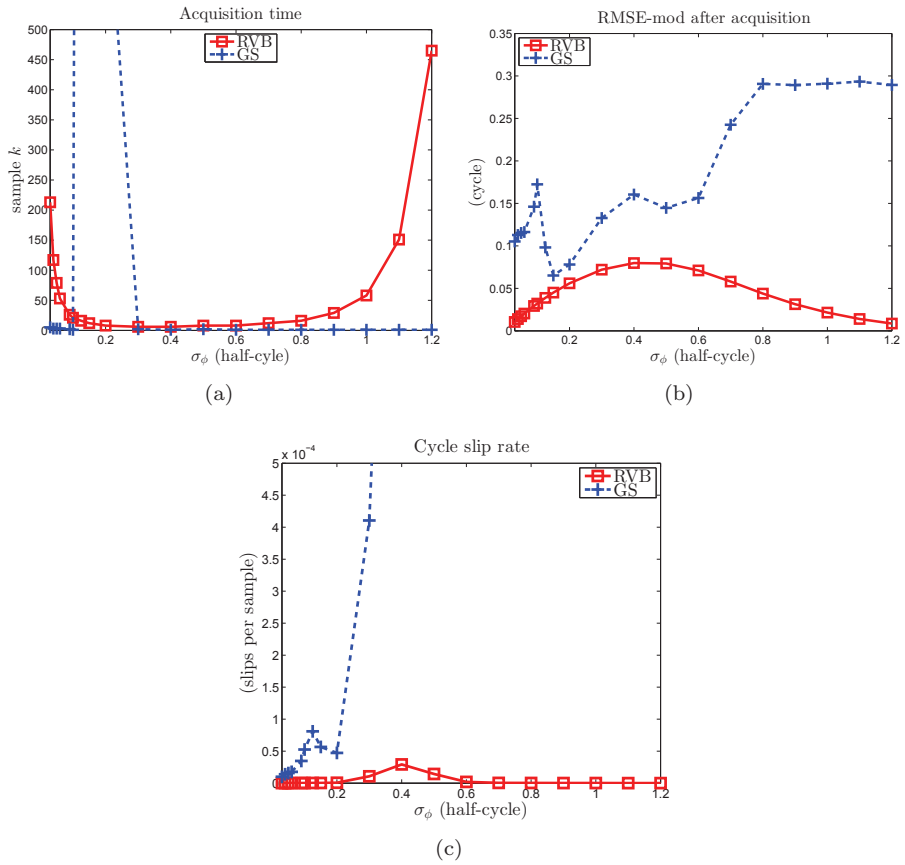

Figure 7: Performance of the proposed RVB estimator and the GS estimator of [26] for a phase-step process. $|\varrho| \approx 0.75$ (e.g., SNR=30 dB, $\rho = 0.75$), $\gamma = 1.25$, $\phi_0 = .25$ cycle, $\dot{\phi}_0 = 0$ cycle/sample. (a) Acquisition time. (b) RMSE-mod after acquisition. (c) Cycle slip rate.

power σ_ϕ^2 is chosen for each estimator among the range of values that minimize the cycle slip rate (graph not depicted here), e.g., $\sigma_\phi = 0.3$ h.c. for the RVB estimator and $\sigma_\phi = 0.1$ h.c. for the GS estimator. As can be observed, on this specific track, only the RVB algorithm succeeds in estimating the absolute phase. Indeed, it does not endure any cycle slip whereas the GS estimator is subject to two cycle slips between the 5th and 10th second of the tracking.

5. Conclusion

In this paper we have proposed a signal model suited for correlated dual-frequency measurements having a slow time varying phase. Accordingly, a Bayesian filtering technique has been described to estimate sequentially the absolute phase of the measurements. The method is obtained by applying a

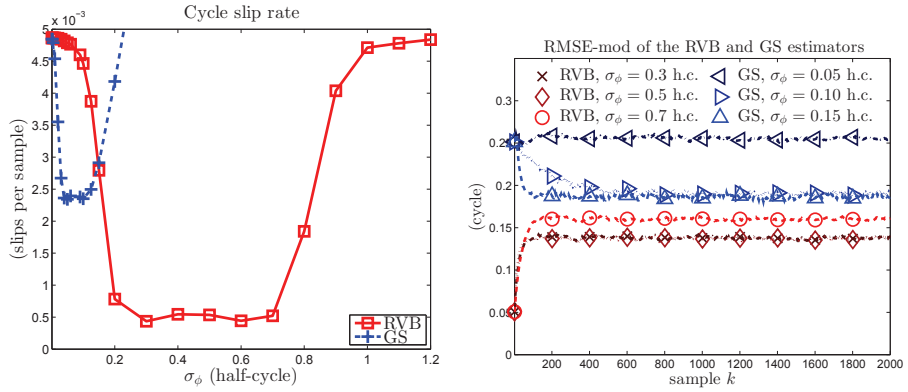

Figure 8: Performance of the proposed RVB estimator and the GS estimator of [26] for a phase-ramp process. $|\varrho| \approx .25$ (e.g., SNR=30 dB, $\rho = 0.25$), $\gamma = 1.25$, $\phi_0 = 0$ cycle, $\dot{\phi}_0 = .005$ cycle/sample. (a) Cycle slip rate. (b) RMSE-mod as a function of the time index.

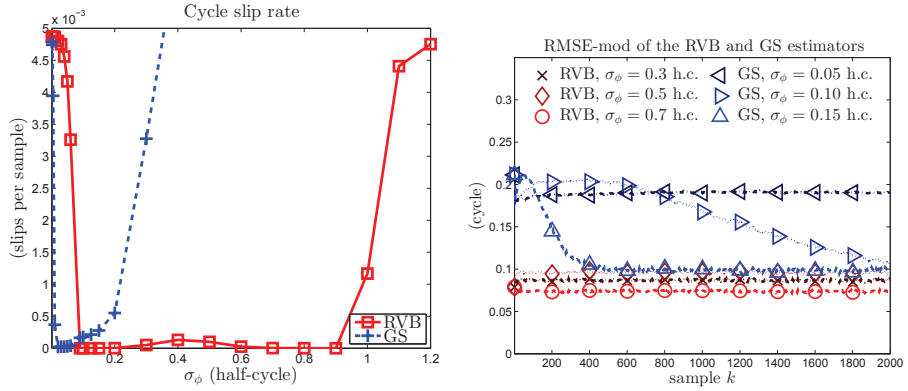

Figure 9: Performance of the proposed RVB estimator and the GS estimator of [26] for a phase-ramp process. $|\varrho| \approx .5$ (e.g., SNR=30 dB, $\rho = 0.5$), $\gamma = 1.25$, $\phi_0 = 0$ cycle, $\dot{\phi}_0 = .005$ cycle/sample. (a) Cycle slip rate. (b) RMSE-mod as a function of the time index.

local variational Bayes approximation in the filtering problem. The resulting filtering distribution has a simple functional form which consists of the product of a von Mises pdf with a Gaussian pdf. Respectively, we have derived in closed form the minimum mean square error estimator. More precisely, the latter, denoted as the RVB estimator, is obtained via a nonlinear updating equation. Numerical simulations have shown that the RVB filter can be advantageous over a more conventional approach, namely a Gaussian sum approximation, in terms of RMSE and cycle slip rate especially at low SNR and/or for low correlation coefficient. Additionally, the tuning of the process noise power has been proven

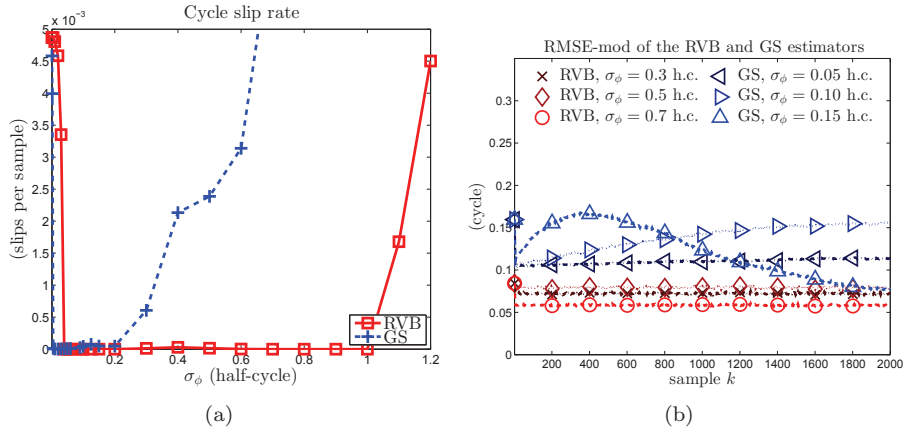

Figure 10: Performance of the proposed RVB estimator and the GS estimator of [26] for a phase-ramp process. $|\varrho| \approx 0.75$ (e.g., SNR=30 dB, $\rho = 0.75$), $\gamma = 1.25$, $\phi_0 = 0$ cycle, $\dot{\phi}_0 = .005$ cycle/sample. (a) Cycle slip rate. (b) RMSE-mod as a function of the time index.

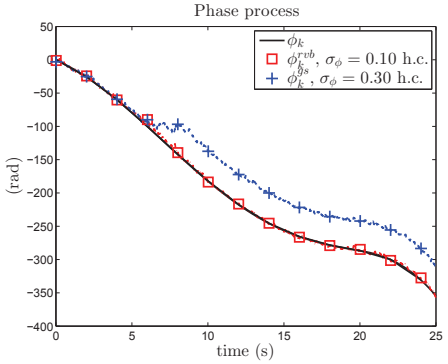

Figure 11: Phase process with a realistic dynamics for GNSS applications (true phase, proposed RVB estimator with $\sigma_\phi = 0.3$ h.c., GS estimator of [26] with $\sigma_\phi = 0.1$ h.c.). $|\varrho| = 0.45$ (e.g., $\rho = 0.9$ and SNR=0 dB), $\gamma \approx 1.28$ (a cycle slip is equal to ≈ 22 rad).

to be less critical for the proposed RVB than for the Gaussian sum estimator.

In future work, it could be of interest to adapt the proposed technique to higher order dynamics and to investigate the more general case of multifrequency signals (i.e., more than two frequencies). Furthermore, the technique could be extended so as to estimate jointly the phase process with the (so-far) assumed known parameters particularly the signal-to-noise ratio and the correlation coefficient. This way, a complete adaptive estimation scheme could be designed. In any event, note that according to the domain of application, the proposed Bayesian model may require some refinement (e.g., in case of channel dependent power) to fit more accurately the received signal.

Appendix A. Modes of the VB filtering distribution

The number of modes of the RVB filtering distribution (15b) and their respective location can be found via a conventional albeit tedious study of function. Due to space limitations, only results are conveyed hereafter with the notation $\delta_k = \beta_k \tilde{\gamma}^2 \sigma_\phi^2$.
If $\delta_k \leq 1$, the pdf is unimodal:

- If $\hat{\phi}_{k-1}^{\text{rvb}} \neq \hat{\psi}_k^{\text{mml}} \mod (\pi/\tilde{\gamma})$, the unique mode is in the open interval with endpoints $\hat{\phi}_{k-1}^{\text{rvb}}$ and $\hat{\psi}_k^{\text{mml}} + 2p_0\pi/\tilde{\gamma}$ where $p_0 = \arg\min_{p\in\mathbb{Z}} \left|\hat{\psi}_k^{\text{mml}} + 2p\pi/\tilde{\gamma} - \hat{\phi}_{k-1}^{\text{rvb}}\right|$.
- Otherwise, the unique mode is $\hat{\phi}_{k-1}^{\text{rvb}}$.

If $\delta_k > 1$, the pdf is uni- or multimodal:

- If $\hat{\phi}_{k-1}^{\text{rvb}} \neq \hat{\psi}_k^{\text{mml}} \mp \tilde{\gamma}^{-1}\left[\sqrt{\delta_k^2 - 1} + \arccos(-\delta_k^{-1})\right] \mod (2\pi/\tilde{\gamma})$ there are $\ell_0 - n_0$ modes and the nth mode for $n = 1, \ldots, \ell_0 - n_0$ is located in the open interval
$$]\theta_0, \Theta_0[+ \frac{2\pi}{\tilde{\gamma}}(\ell_0 + n)$$
where
$$\begin{aligned}
\theta_0 &= \hat{\psi}_k^{\text{mml}} - \frac{1}{\tilde{\gamma}} \arccos(-\delta_k^{-1}) \\
\Theta_0 &= \hat{\psi}_k^{\text{mml}} + \frac{1}{\tilde{\gamma}} \arccos(-\delta_k^{-1}) \\
\ell_0 &= \lfloor \tilde{\gamma}/(2\pi) s(\theta_0) \rfloor \\
n_0 &= \lfloor \tilde{\gamma}/(2\pi) s(\Theta_0) \rfloor
\end{aligned}$$
with $\lfloor\rfloor$ the floor function and $s(.)$ the function defined by
$$s(\phi_k) = \frac{\delta_k}{\tilde{\gamma}} \sin\left(\tilde{\gamma}[\hat{\psi}_k^{\text{mml}} - \phi_k]\right) - \phi_k + \hat{\phi}_{k-1}^{\text{rvb}}.$$
- Otherwise, three "degenerated" cases can easily be defined from the latter case where one or two modes are inflection points.

Appendix B. Derivation of $\hat{\phi}_1^{\text{rvb}}$

In this Appendix we derive the expression (17) of the RVB estimator for $k = 1$. Our derivations use extensively the expression of the Fourier series [28, p.376,9.6.34]
$$\exp\{\beta\cos(x)\} = I_0\{\beta\} + 2\sum_{q=1}^{+\infty} I_q\{\beta\}\cos(qx) \tag{B.1}$$

where $I_q\{x\} = 1/\pi \int_0^\pi e^{x\cos(\theta)}\cos(q\theta)d\theta$ is the modified Bessel function of the first kind and of order q.

Using (16) and (14b), the RVB estimator at $k = 1$ can be expressed as

$$\hat{\phi}_1^{\text{rvb}} = \frac{\int_{\phi_1} \phi_1 f(\phi_1) \exp\left\{\beta_1 \cos(\tilde{\gamma}[\hat{\psi}_1^{\text{mml}} - \phi_1])\right\} d\phi_1}{\int_{\phi_1} f(\phi_1) \exp\left\{\beta_1 \cos(\tilde{\gamma}[\hat{\psi}_1^{\text{mml}} - \phi_1])\right\} d\phi_1}. \tag{B.2}$$

The denominator of (B.2), denoted as d_1 corresponds to the normalizing constant of a von Mises pdf [25, p.36], so that $d_1 = 2\pi I_0\{\beta_1\}/\tilde{\gamma}$.
Using (B.1), the numerator of (B.2), denoted as n_1, can be rewritten as

$$n_1 = \int_{-\frac{\pi}{\tilde{\gamma}}}^{\frac{\pi}{\tilde{\gamma}}} \phi_1 \left[I_0\{\beta_1\} + 2\sum_{q=1}^{+\infty} I_q\{\beta_1\}\cos(q\tilde{\gamma}[\hat{\psi}_1^{\text{mml}} - \phi_1])\right] d\phi_1. \tag{B.3}$$

Using an integration by parts on the second term leads to

$$n_1 = -\frac{4\pi}{\tilde{\gamma}^2}\sum_{q=1}^{+\infty}(-1)^q \frac{I_q\{\beta_1\}\sin(q\tilde{\gamma}\hat{\psi}_1^{\text{mml}})}{q}$$

which allows to recover the expression (17).

Appendix C. Derivation of $\hat{\phi}_k^{\text{rvb}}$, $k \geq 1$

In this Appendix we derive the expression (18) of the RVB estimator for $k > 1$. Using (16) and (15b), the RVB estimator can be formulated as

$$\hat{\phi}_k^{\text{rvb}} = \frac{\int_{\phi_k} \phi_k \exp\left\{\beta_k \cos(\tilde{\gamma}[\hat{\psi}_k^{\text{mml}} - \phi_k]) - \frac{(\phi_k - \hat{\phi}_{k-1}^{\text{rvb}})^2}{2\sigma_\phi^2}\right\} d\phi_k}{\int_{\phi_k} \exp\left\{\beta_k \cos(\tilde{\gamma}[\hat{\psi}_k^{\text{mml}} - \phi_k]) - \frac{(\phi_k - \hat{\phi}_{k-1}^{\text{rvb}})^2}{2\sigma_\phi^2}\right\} d\phi_k}.$$

The numerator and the denominator of the former expression are denoted respectively as n_k and d_k, i.e., $\hat{\phi}_k^{\text{rvb}} \triangleq n_k/d_k$. Using results from [34, p. 1653], the denominator d_k can be expressed as

$$d_k = \sqrt{2\pi}\sigma_\phi \left[I_0\{\beta_k\} + 2\sum_{q=1}^{+\infty} I_q\{\beta_k\} e^{-\frac{\sigma_\phi^2 q^2 \tilde{\gamma}^2}{2}} \cos\left(q\tilde{\gamma}[\hat{\psi}_k^{\text{mml}} - \hat{\phi}_{k-1}^{\text{rvb}}]\right)\right]. \tag{C.1}$$

Applying then the Parseval's theorem to the numerator n_k, one has

$$n_k = \int_\nu \mathcal{F}\left\{e^{\beta_k \cos(\tilde{\gamma}[\hat{\psi}_k^{\text{mml}} - \phi_k])}\right\}(\nu)\mathcal{F}^*\left\{\phi_k e^{-\frac{(\phi_k - \hat{\phi}_{k-1}^{\text{rvb}})^2}{2\sigma_\phi^2}}\right\}(\nu)d\nu \tag{C.2}$$

where $\mathcal{F}\{g\}(\nu)$ is the Fourier transform of the function g at the frequency point ν. Using standard properties of the Fourier transform and the Fourier series (B.1), the first term involved in (C.2) can be expressed as

$$\mathcal{F}\left\{e^{\beta_k \cos(\tilde{\gamma}[\hat{\psi}_k^{\mathrm{mml}}-\phi_k])}\right\}(\nu) = I_0\{\beta_k\}\delta(\nu) + e^{-j2\pi\nu\hat{\psi}_k^{\mathrm{mml}}}\sum_{q=1}^{+\infty} I_q\{\beta_k\}\left[\delta(\nu - q\frac{\tilde{\gamma}}{2\pi}) + \delta(\nu + q\frac{\tilde{\gamma}}{2\pi})\right] \quad \text{(C.3)}$$

where $\delta(\nu)$ is the Delta Dirac function. The second term is obtained by integration by parts

$$\mathcal{F}\left\{\phi_k e^{-\frac{(\phi_k-\hat{\phi}_{k-1}^{\mathrm{rvb}})^2}{2\sigma_\phi^2}}\right\}(\nu) = \sqrt{2\pi}\sigma_\phi\left[\hat{\phi}_{k-1}^{\mathrm{rvb}} - j2\pi\sigma_\phi^2\nu\right]e^{-j2\pi\nu\hat{\phi}_{k-1}^{\mathrm{rvb}}}e^{-2\pi^2\sigma_\phi^2\nu^2}. \quad \text{(C.4)}$$

Plugging then (C.3) and (C.4) in (C.2) yields

$$n_k = \sqrt{2\pi}\sigma_\phi\left[I_0\{\beta_k\}\hat{\phi}_{k-1}^{\mathrm{rvb}} + 2\sum_{q=1}^{+\infty} I_q\{\beta_k\}e^{-\frac{\sigma_\phi^2 q^2\tilde{\gamma}^2}{2}} \left\{\hat{\phi}_{k-1}^{\mathrm{rvb}}\cos\left(q\tilde{\gamma}[\hat{\psi}_k^{\mathrm{mml}} - \hat{\phi}_{k-1}^{\mathrm{rvb}}]\right) + \sigma_\phi^2\tilde{\gamma}\,q\,\sin\left(q\tilde{\gamma}[\hat{\psi}_k^{\mathrm{mml}} - \hat{\phi}_{k-1}^{\mathrm{rvb}}]\right)\right\}\right]. \quad \text{(C.5)}$$

Finally, combining (C.1) and (C.5) the expression (18) can be recovered.

Acknowledgements

The work of S. Roche is supported by the French space agency CNES and by Thales Alenia Space.

The authors are grateful to Thales Alenia Space for providing the synthetic GNSS data.

References

[1] P. Rosen, S. Hensley, I. Joughin, F. Li, S. Madsen, E. Rodriguez, R. Goldstein, Synthetic aperture radar interferometry, Proc. IEEE 88 (3) (2000) 333 –382.

[2] M. Skolnik (Ed.), Radar Handbook, 3rd Edition, McGraw-Hill, 2008.

[3] E.D. Kaplan, C.J. Hegarty (Eds.), Understanding GPS: Principles and Applications, 2nd Edition, Artech House, 2006.

[4] K. Itoh, Analysis of the phase unwrapping algorithm, Appl. Opt. 21 (14) (1982) 2470.

[5] G. Ascheid, H. Meyr, Cycle slips in phase-locked loops: a tutorial survey, IEEE Trans. Commun. 30 (1982) 2228–2241.

[6] J.M.N. Leitão, J.M.F. Moura, Acquisition in phase demodulation: application to ranging in radar/sonar systems, IEEE Trans. Aerosp. Electron. Syst. 31 (2) (1995) 581–599.

[7] J.M.N. Leitão, M.A.T. Figueiredo, Absolute phase image reconstruction: a stochastic nonlinear filtering approach, IEEE Trans. Image Process. 7 (6) (1998) 868–882.

[8] J.-F. Giovannelli, J. Idier, R. Boubertakh, A. Herment, Unsupervised frequency tracking beyond the Nyquist frequency using Markov chains, IEEE Trans. Signal Process. 50 (12) (2012) 2905–2914.

[9] J. Bioucas-Dias, V. Katkovnik, J. Astola, Multi-frequency phase unwrapping from noisy data: adaptive local maximum likelihood approach, in: A.-B. Salberg, J. Hardeberg, R. Jenssen (Eds.), Image Analysis, Vol. 5575 of Lecture Notes in Computer Science, Springer Berlin Heidelberg, 2009, pp. 310–320.

[10] H. Yu, Z. Li, Z. Bao, A cluster-analysis-based efficient multibaseline phase-unwrapping algorithm, IEEE Trans. Geosci. and Remote Sens., on 49 (1) (2011) 478–487.

[11] R. Tigrek, W.J.A. De Heij, P. Van Genderen, OFDM signals as the radar waveform to solve Doppler ambiguity, IEEE Trans. Aerosp. Electron. Syst. 48 (1) (2012) 130–143.

[12] G. Trunk, S. Brockett, Range and velocity ambiguity resolution, in: Radar Conference, 1993, Record of the 1993 IEEE National, 1993, pp. 146–149.

[13] P. Henkel, K. Giger, C. Guenther, Multifrequency, multisatellite vector phase-locked loop for robust carrier tracking, IEEE J. Select. Top. Signal Process. 3 (4) (2009) 674–681.

[14] C. Gernot, K. O'Keefe, G. Lachapelle, Assessing three new GPS combined L1/L2C acquisition methods, IEEE Trans. Aerosp. Electron. Syst. 47 (3) (2011) 2239 –2247.

[15] N.I. Ziedan, Multi-frequency combined processing for direct and multipath signals tracking based on particle filtering, in: Proceedings of International Technical Meeting of the Satellite Division of the Institute of Navigation, Portland, OR, 2011, pp. 1090–1101.

[16] D. Droeschel, D. Holz, S. Behnke, Multi-frequency phase unwrapping for time-of-flight cameras, in: Intelligent Robots and Systems (IROS), 2010 IEEE/RSJ International Conference on, 2010, pp. 1463–1469.

[17] F.D. Nunes, J.M.N. Leitão, F. M. G. Sousa, Nonlinear filtering in GNSS pseudorange dynamics estimation combining code delay and carrier phase, IEEE J. Select. Top. Signal Process. 3 (4) (2009) 639–650.

[18] F. Le Chevalier, Radar non ambigü à large bande, 1996.

[19] K. Kastella, R. Mudumbai, T. Stevens, Frequency estimation in the presence of cycle slips: filter banks and error bounds for phase unwrapping, in: Proceedings of IEEE Statistical Signal Processing Workshop, Ann Arbor, MI, 2012.

[20] V. Smídl, A. Quinn, Variational Bayes filtering, IEEE Trans. Signal Process. 56 (10) (2008) 5020–5030.

[21] B. Ristic, S. Arulampalam, N. Gordon, Beyond the Kalman Filter: Particle Filters for Tracking Applications, Artech House, 2004.

[22] J. Dias, J. Leitão, InSAR phase unwrapping: a Bayesian approach, in: IEEE Int. Geoscience and Remote Sensing Symposium, vol. 1, 2001, pp. 396–400.

[23] J.-S. Lee, A. Miller, K. Hoppel, Statistics of phase difference and product magnitude of multi-look processed Gaussian signals, Waves in Random Media 4 (3) (1994) 307–319.

[24] B.D.O. Anderson, J. B. Moore, Optimal Filtering, Prentice-Hall, 1979.

[25] K.V. Mardia, P.E. Jupp, Directional Statistics, in: Wiley Series in Probability and Statistics, Wiley, 2000.

[26] J. Moura, A. Baggeroer, Phase unwrapping of signals propagated under the arctic ice crust: a statistical approach, IEEE Trans. Acoust. Speech Signal Process. 36 (5) (1988) 617–630.

[27] D. Alspach, H. Sorenson, Nonlinear Bayesian estimation using Gaussian sum approximations, IEEE Trans. Autom. Control 17 (4) (1972) 439–448.

[28] M. Abramowitz, I. Stegun, Handbook of Mathematical Functions, Dover Publications, 1965.

[29] F. Charles, W. Lindsey, Some analytical and experimental phase-locked loop results for low signal-to-noise ratios, Proc. IEEE 54 (9) (1966) 1152–1166.

[30] A. J. Viterbi, Phase-locked loop dynamics in the presence of noise by Fokker-Planck techniques, Proc. IEEE 51 (1963) 1737–1753.

[31] S.M. Brunt, M. Darnell, M. Grayson, Cycle-slipping probability of first-order phase-locked loop using transient analysis, IEE Proc. Commun. 144 (5) (1997) 357–360.

[32] C.M. Chie, W. Lindsey, Phase-locked loops: applications, performance measures, and summary of analytical results, Phase-Locked Loops, IEEE Press, Piscataway, NJ.

[33] D. Amos, A subroutine package for Bessel functions of a complex argument and nonnegative order, Technical report, SandiaNational Laboratory, May 1985.

[34] F.D. Nunes, J.M.N. Leitão, A nonlinear filtering approach to estimation and detection in mobile communications, IEEE J. Sel. Areas Commun. 16 (9) (1998) 1649–1659.